Two *Ka*-Band Quasi-Optical Amplifier Arrays

Todd Marshall, *Student Member, IEEE,* Michael Forman, *Student Member, IEEE,* and Zoya Popović, *Senior Member, IEEE*

***Abstract*— Repeatability of performance, thermal properties, and effects of biasing are studied on two Ka-band quasi-optical slot-antenna amplifier arrays, fabricated with commercial monolithic microwave integrated circuits (MMIC's) on aluminum–nitride substrates. The unit cells are arranged in a 6 × 6 triangular lattice to suppress sidelobes. The amplifier arrays have small-signal gains relative to a free-space through of 2.1 dB at 31.02 GHz and 6.5 dB at 31.40 GHz. The average small-signal gain contributed by the MMIC's is 10 dB. In saturation, the arrays deliver 89 W effective isotropic radiated power (EIRP) or 0.3 W output power at 30.40 GHz and 145 W EIRP or 0.5 W output power at 31.15 GHz.**

***Index Terms*— Aluminum nitride, amplifier array, free-space power combiner, Ka-band, quasi-optical.**

I. Introduction

THE motivation for quasi-optical amplifier power combining is to obtain watt power levels from solid-state amplifiers at millimeter-wave frequencies while taking advantage of high combining efficiency [1] and graceful degradation [2]. Several researchers have demonstrated Ka-band quasi-optical amplifier arrays: in [3], monolithic-microwave integrated-circuit (MMIC) amplifiers were combined using patch antennas with 4 W of output power and 16 dB of large-signal gain; in [4] and [5], monolithic grid amplifiers, using heterojunction bipolar transistors (HBT's) and pseudomorphic high electron-mobility transistors (pHEMT's), respectively, showed gain up to 60 GHz, and in [6], 1 W of power was obtained in an array mounted in a waveguide.

In this paper, fundamental studies related to the repeatability of array performance; thermal properties of substrate, effect of device biasing, and sensitivity to fabrication tolerances are presented. The studies are performed on two experimental Ka-band arrays (referred to as Arrays A and B) of nearly identical RF architectures. The arrays differ only in the implementation of the biasing network and substrate metallization thickness.

II. Array Amplifier Design

The quasi-optical amplifier schematic is shown in Fig. 1. The input slot antennas receive power from an incident vertically polarized plane wave. In each cell, the received power is coupled onto the 50-Ω coplanar waveguide (CPW) transmission line and is then amplified by a commercial low-cost low-power Alpha AA028P3-00 MMIC driver amplifier. The MMIC amplifier has 19 dB of small-signal gain, and 16 dBm of output power at the 1-dB compression point. The amplified power is reradiated in the horizontal polarization by the output slot antennas and is the coherent combination of all element outputs. Isolation and stability are provided by orthogonal polarization of input and output antennas.

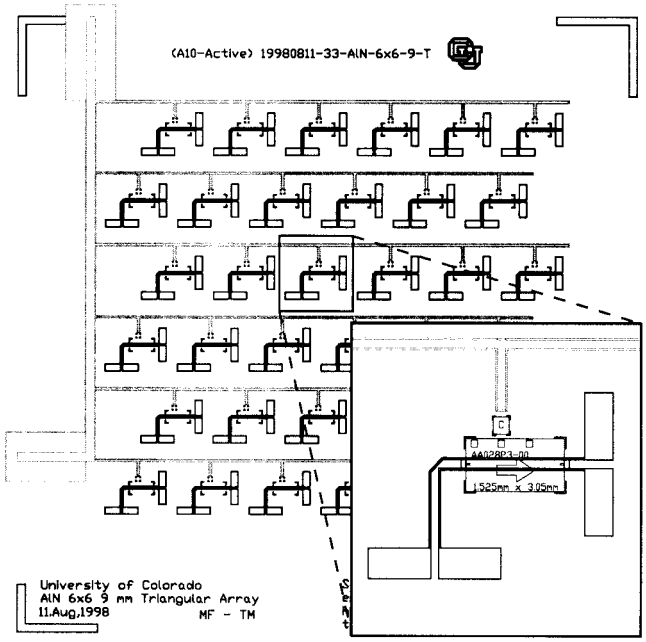

Fig. 1. Schematic of a unit cell within the amplifier array. The unit cells are arranged in a triangular lattice. The slot antennas are orthogonally polarized and are connected to the MMIC by CPW transmission lines. The dc-bias line and blocking capacitor are also shown.

A. Thermal Modeling

The choice of substrates is constrained by the 125 °C maximum operating temperature of the MMIC. Thermal gradients on substrates during operation are approximated with a simple analytical model of heat conduction. The model assumes a uniform heat flux under each MMIC and a uniform temperature of 25 °C along the edge of the substrate. The substrate dimensions are 7.62 cm × 7.62 cm × h, where h varies from 254 to 406 μm, depending on the commercial availability of the substrate. An array has 36 unit cells spaced 9 mm ($0.9\lambda_0$) apart. The 36 Alpha AA028P3-00 MMIC's produce $P_h = 33$ W of heat. The maximum expected temperatures based on the conduction model for diamond, aluminum nitride (AlN), and Rogers TMM6 substrates are given in Table I.

The diamond substrate has the lowest thermal gradient. The unrealistic maximum temperature calculated for the TMM6 substrate demonstrates the limitation of any model based solely on heat conduction. However, at higher temperatures,

Manuscript received March 26, 1999; revised July 9, 1999. This work was supported by Lockheed-Martin under the Defense Advanced Research Projects Agency MAFET3 Program.

The authors are with the Department of Electrical and Computer Engineering, University of Colorado, Boulder, CO 80309-0425 USA.

Publisher Item Identifier S 0018-9480(99)08457-4.

TABLE I
THEORETICAL MAXIMUM TEMPERATURE BASED ON CONDUCTION ONLY

Substrate	h (μm)	k (W/(m K))	P_h (W)	T_{max} (°C)
Diamond	406.4	2000	33	30.3
AlN	254	170	33	124
TMM6	381	0.7	33	15000

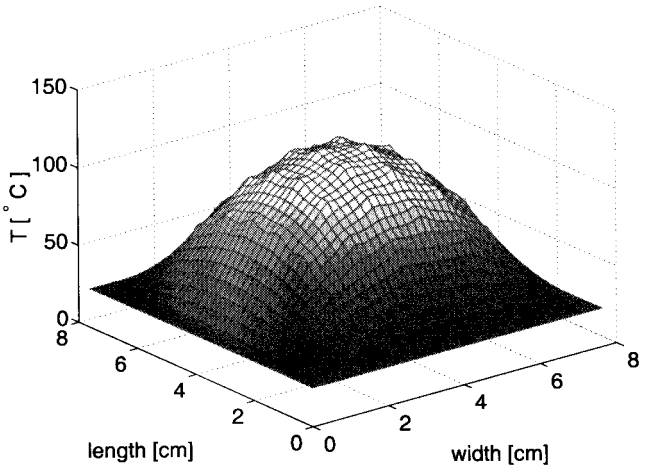

Fig. 2. Theoretical temperature on the surface of the AlN substrate is plotted as a function of position. The spikes in the temperature distribution are due to the finite area of individual MMIC's.

cooling is dominated by convection and radiation that will decrease the maximum temperature, making these numbers an absolute maximum. The AlN substrate is chosen over diamond because its 100 °C thermal gradient (Fig. 2) meets the MMIC temperature requirements and the substrate is comparatively inexpensive. The AlN substrate is 254 μm thick with a relative permittivity of 8.6.

B. Mutual Coupling of Array Elements

HP Momentum was used to design the CPW transmission line, the 90° compensated bend, and the 50-Ω slot antenna. The second-resonance slot antenna is 4.15-mm long and 0.9-mm wide, and has a modeled return loss of 50 dB at 33 GHz with a 13% 2 : 1 VSWR bandwidth.

HP Momentum simulations were performed to study coupling between slot antennas and bias lines to determine the minimum size of the unit cell. A $0.9\lambda_0$ unit cell is chosen to keep coupling between the orthogonally polarized input and output antennas below -20 dB (lower than the maximum MMIC gain) for stability. The dc-bias lines are oriented perpendicular to the output antennas to minimize coupling (Fig. 3).

C. Biasing

There is dc-voltage variation across the array due to ohmic losses in the thin bias lines. The biasing network is modeled as a resistive ladder network consisting of series $R_{\rm bias}$ and shunt $R_{\rm MMIC}$ resistors (Fig. 4). The variables $R_{\rm bias}$ and $R_{\rm MMIC}$ represent the resistance of the unit-cell bias line and the resistance of the internal MMIC biasing circuitry, respectively.

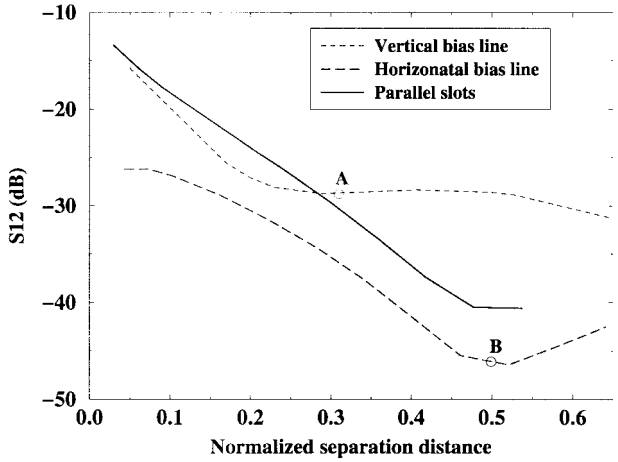

Fig. 3. Coupling is calculated as a function of normalized separation distance. The normalized separation distance is the shortest distance between the two elements divided by the slot antenna length. The circles correspond to the normalized distances used in the final array design.

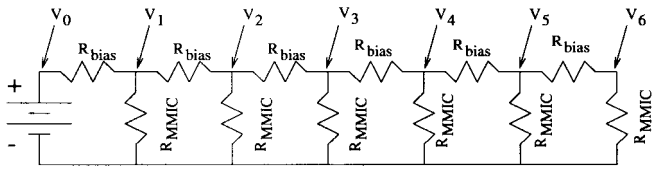

Fig. 4. Resistive ladder network diagram used to calculate MMIC bias levels within the array.

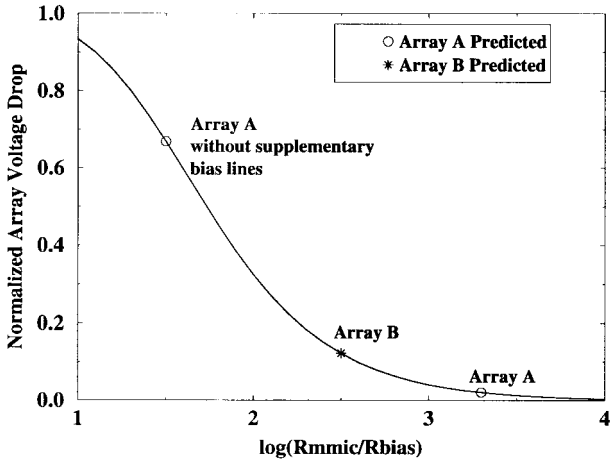

Fig. 5. Normalized array voltage drop as a function of $R_{\rm MMIC}/R_{\rm bias}$.

The bias voltage along a row at the $(k+1)$ unit cell is given by

$$V_{k+1} = \frac{R_{N-k-1}}{R_{\rm bias} + R_{N-k-1}} V_k, \tag{1}$$

where

$$R_j = \left[\frac{1}{R_{\rm MMIC}} + \frac{1}{R_{\rm bias} + R_{j-1}} \right]^{-1}. \tag{2}$$

The number of unit cells in a row is $N = 6$, $j = 1$ to $N-1$, and $k = 0$ to $N-1$. $k = 0$ corresponds to the supply voltage V_0 and $R_0 \equiv R_{\rm MMIC}$. Equations (1) and (2), expressed as a function of the ratio $R_{\rm MMIC}/R_{\rm bias}$, show that the bias voltage variation over an array may be substantial (Fig. 5).

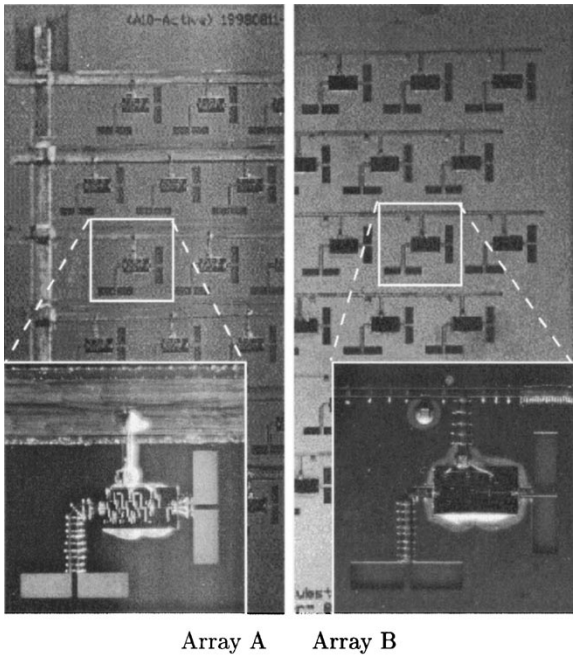

Fig. 6. Arrays A and B with corresponding unit cells enlarged. The size of the unit cell is 9 mm $\times$ 9 mm.

III. Fabrication

Arrays A and B, shown in Fig. 6, were fabricated using photolithography from the same mask. The MMIC's and capacitors were bonded with silver epoxy. Each of the unit cells in both arrays has 25 gold bond wires in identical configurations. The bond wires provide connections between the MMIC pads, capacitor pads, and array metallization, as well as air bridges along the CPW lines to prevent slot modes.

Arrays A and B differ in metal thickness and bias line configuration. The substrate used for Array A has 4 μm of gold, which results in a low $R_{\mathrm{MMIC}}/R_{\mathrm{bias}}$ ratio. A supplementary bias line network consisting of insulating adhesive mylar and copper tape was added to compensate. The substrate for Array B has 4.3 μm of copper with an additional 2-μm layer of electroplated gold. The thicker metal increases $R_{\mathrm{MMIC}}/R_{\mathrm{bias}}$, thus decreasing the dc-bias network voltage variation. Array B has additional airbridges and a capacitor along the bias line.

IV. Experimental Results

In this section, results from experiments performed on the two arrays are presented. In particular, the following are discussed: thermal measurements, elements of the array, small-signal gain, saturated power, far-field patterns, and measurement of bias variations.

A. Thermal Measurements

With the arrays mounted vertically and under small-signal excitation, natural heat convection leads to measured steady-state temperatures of 69 °C and 62 °C for Arrays A and B, respectively. Employing forced-convective cooling using two fans with a flow of 1 m^3/min, the maximum steady-state temperatures for Arrays A and B dropped to 39 °C and 38 °C, respectively. Natural convection is sufficient to keep the MMIC's below their maximum operating temperature in small-signal operation.

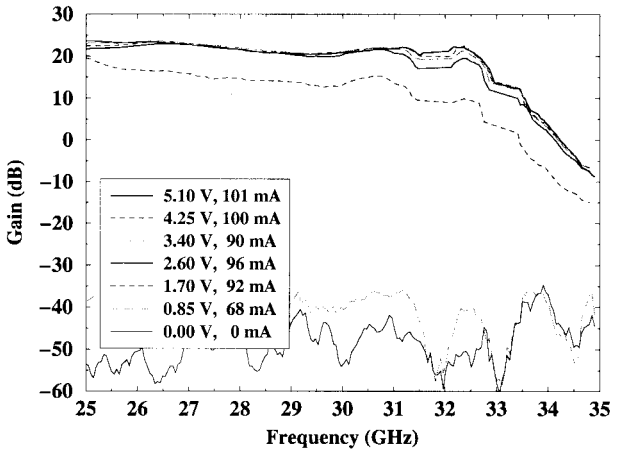

Fig. 7. Measured gain of the Alpha AA028P3-00 MMIC at various bias points.

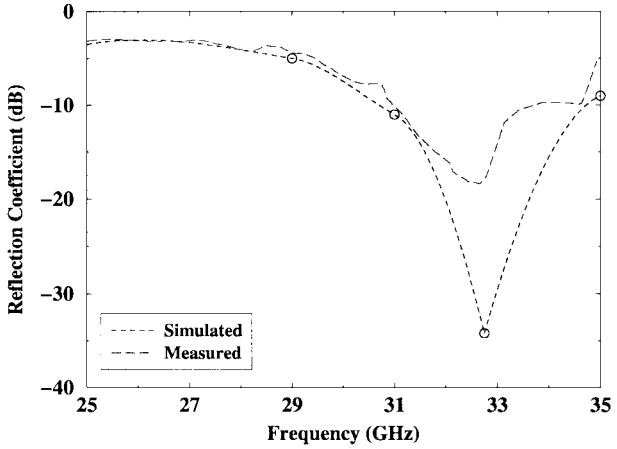

Fig. 8. Simulated and measured response of the slot antenna. HP Momentum was used for the simulation.

B. Elements of the Arrays

To gauge the accuracy of the simulations, various individual array components were fabricated on a separate AlN substrate for characterization. A Cascade probe station and ground–signal–ground (GSG) CPW probes are used to measure the circuits, using a thru-reflection line (TRL) calibration set also fabricated on the AlN substrate. The components of interest are the CPW line and 90° compensated bend, the Alpha MMIC, and the slot antenna. Measurements show that the lines and bends perform as simulated without unexpected losses or mismatches. The measured gain of one of the MMIC's at 31 GHz is shown in Fig. 7. The measured resonance of the slot antenna is 32.6 GHz and is shifted 150 MHz (0.5%) from the simulated value of 32.75 GHz (Fig. 8). The slot antenna has a measured and simulated bandwidth of 3.7 (11%) and 4.3 GHz (13%). The antenna simulation includes an increase in antenna and CPW dimensions resulting from overetching in the fabrication process.

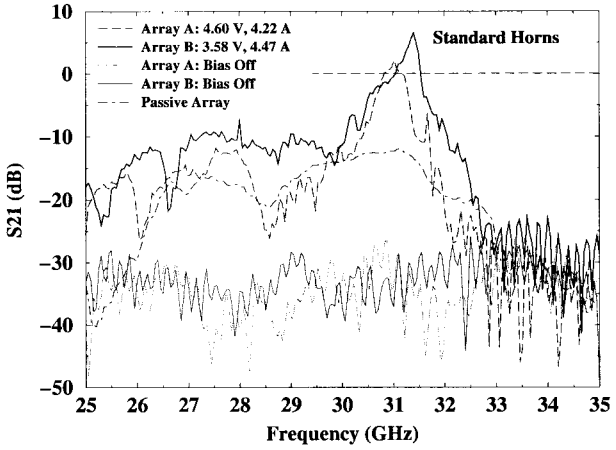

(a)

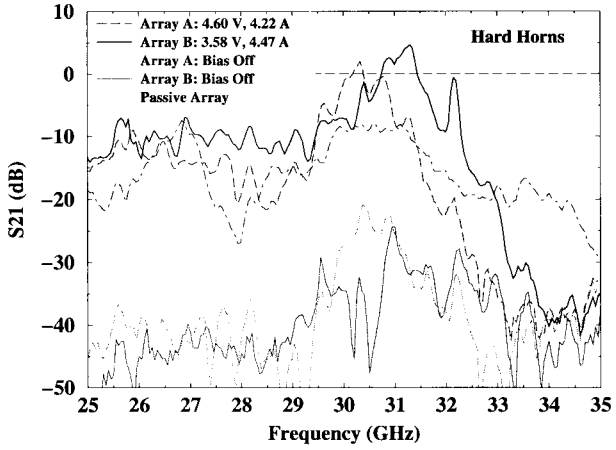

(b)

Fig. 9. Small-signal gain measurements with: (a) standard horns and (b) hard horns. Measurements are with respect to a through calibration.

C. Small Signal

The characterization of the arrays is performed with the following three measurements:

1) small-signal far-field gain measurement with standard horns;
2) small-signal near-field gain measurement with hard horns;
3) large-signal far-field power measurement with standard horns.

For the small-signal far-field measurement, two 21.5-dB cross-polarized standard horn antennas are placed $60\lambda_0$ from either side of the array. Measurements are performed with an HP8510C vector network analyzer calibrated to a free-space through. In theory, tuned polarizers should increase the gain of the array by 6 dB by enforcing unidirectional radiation of the slot antennas. Measurements place the actual increase in gain at 3 dB. Fig. 9(a) shows the measured gain of the passive and active arrays with respect to a through calibration. Measurements are summarized in Table II(a). The average gain contributed by the MMIC amplifiers is 10 dB.

Near-field small-signal gain measurements are performed in a similar fashion using two cross-polarized hard-horn antennas

TABLE II
MEASURED SMALL-SIGNAL RESPONSE WITH: (a) STANDARD HORNS AND (b) HARD HORNS. BW INDICATES THE RANGE OVER WHICH THE ARRAYS HAVE GAIN. G_a IS WITH RESPECT TO A PASSIVE ARRAY

Array	freq (GHz)	Gain (dB)	BW (GHz)	On/Off Ratio (dB)	G_a (dB)
A	31.02	2.1	0.34	34	10
B	31.40	6.5	0.50	38	14

(a)

Array	freq (GHz)	Gain (dB)	BW (GHz)	On/Off Ratio (dB)	G_a (dB)
A	30.32	2.0	0.22	25	10
B	31.30	4.7	0.70	35	12

(b)

TABLE III
MEASUREMENT RESPONSE WITH STANDARD HORNS

Array	freq (GHz)	EIRP (dBm)	EIRP (W)	P_t (dBm)	P_t (mW)
A	30.40	49.5	89	25	316
B	31.15	51.6	145	27.1	513

$6\lambda_0$ from the array. The hard-horn antennas provide a uniform field distribution with amplitude and phase variations of only ± 1 dB and 80° over 98% of the horn aperture [7]. The small-signal hard-horn gain measurements are shown in Fig. 9(b) and summarized in Table II(b).

D. Large Signal

Far-field large-signal power measurements, are performed with standard horns placed $25\lambda_0$ from the array. In place of the network analyzer, an HP83640A synthesized sweeper driving a Litton M-762-00 MMPM are used to provide the power required to saturate the arrays. The estimated power incident on the array is 27.7 dBm. An HP437B power meter with a high-frequency power sensor (HP8487A) is used to measure the output power. The effective isotropic radiated power (EIRP) and output powers estimated from measured radiation patterns are summarized in Table III. Measurement accuracies are ± 1 dB. The gain saturation of Arrays A and B is 7.9 and 7.5 dB, respectively.

The saturated output power of the arrays is calculated by dividing the EIRP by the estimated gain of the array. A value of 24.5 dB for the array gain is obtained by both the Krauss approximation and the physical area of the array [8]. The value obtained by Krauss approximation is based upon the large-signal far-field patterns. The radiated power includes the loss of the polarizers, which are an integral part of the QO arrays. By improving polarizer loss, the power could increase by 1.5 dB (or 0.5 and 0.7 W, respectively).

E. Far-Field Patterns

Pattern measurements, are performed using far-field standard-horn antennas $60\lambda_0$ from the array. Measurements are performed with polarizers under large-signal excitation. The theoretical and measured E- and H-plane patterns for

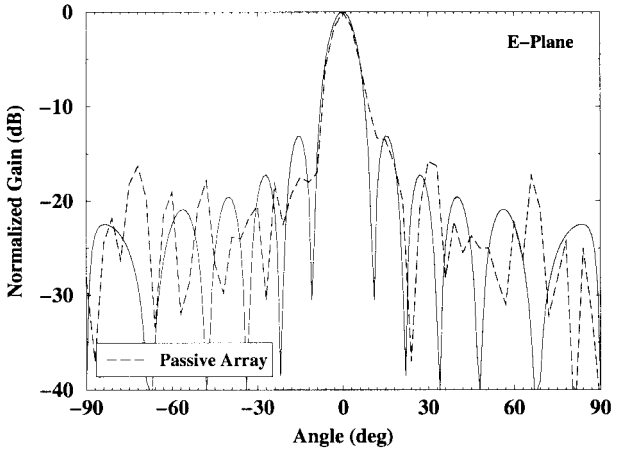

(a)

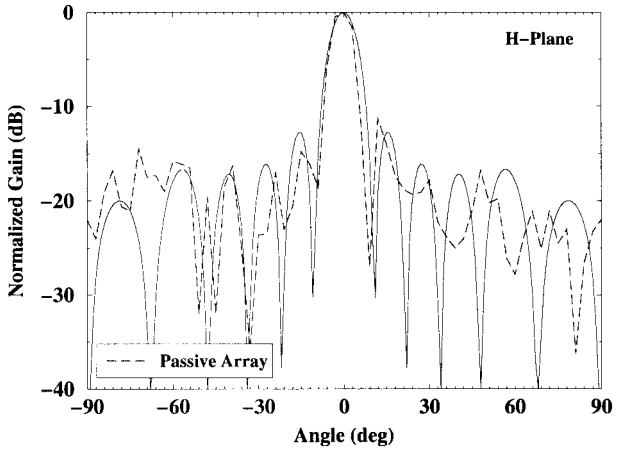

(b)

Fig. 10. (a) Passive E-plane pattern measurement. (b) Passive H-plane pattern measurement. The measurement frequency is 31.4 GHz. The theoretical plot (—) assumes a uniform array.

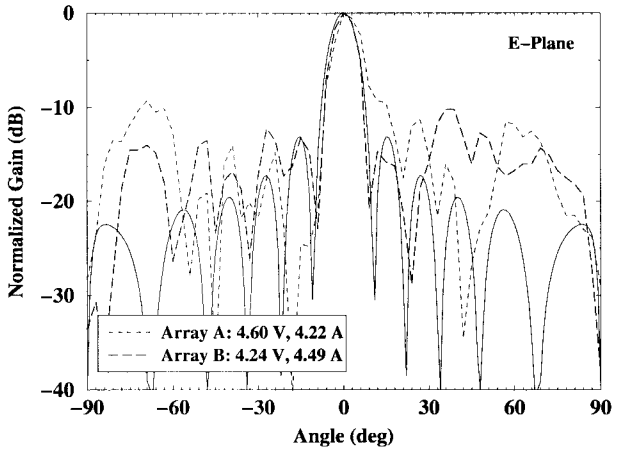

(a)

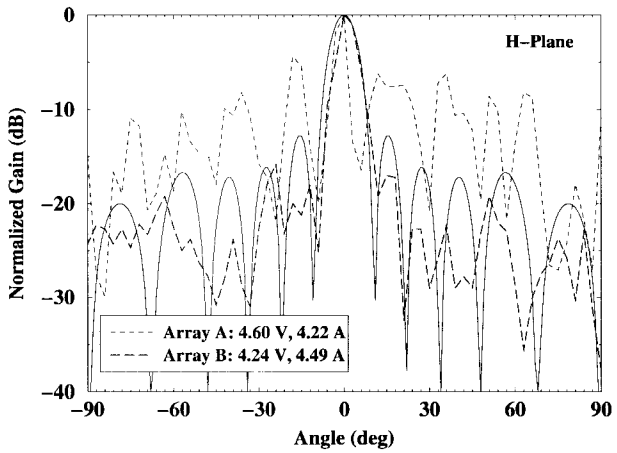

(b)

Fig. 11. (a) Active E-plane pattern measurement. (b) Active H-plane pattern measurement. The measurement frequency is 31.4 GHz. The theoretical plot (—) assumes a uniform array.

the passive and active arrays are shown in Figs. 10 and 11, respectively. Theoretical array patterns are generated by multiplying the array factor by the pattern of the slot antenna. The slot antenna pattern is modeled as a cosine-squared toroid pinched to zero at the substrate.

Although one would expect large sidelobes with a $0.9\lambda_0$ unit cell, sidelobes in both planes are minimized. A triangular array lattice serves to minimize the sidelobes of the array factor in the E-plane. In the H-plane, sidelobes are eliminated due to the toroidal pattern of the slot antenna. It is believed that the difference between theoretical and active patterns is due to a variation of magnitude and phase at the output of the MMIC's, attributed to different MMIC bias points.

F. Bias Variations

Voltage variations are measured across the bias network without RF input. Fig. 12 shows the normalized measured voltage deviation along the bias network at each MMIC due to the bias ladder network. Voltage variations for Array B match the expected values within 5% relative error based on (1) and (2). Array A's vertical voltage uniformity differs from theory due to resistive bus–bar connections [see Fig. 6(a)].

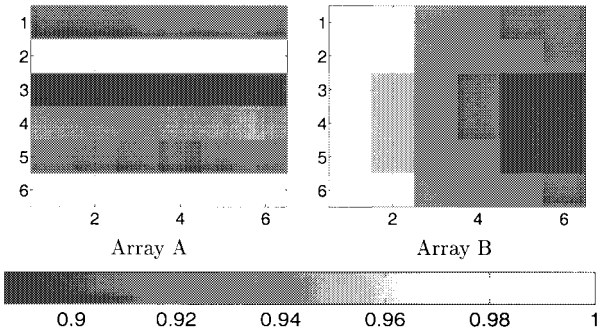

Fig. 12. Measured normalized voltage levels for Arrays A and B.

V. Conclusion

This paper presents a Ka-band quasi-optic power-combining array with 145-W EIRP or 0.5 W of output power at 31 GHz. The active array consists of 36 unit cells with commercial low-power MMIC driver amplifiers. Repeatability of array performance was examined with respect to bias-network variations on two arrays with identical RF architectures, but different biasing networks. The variation of bias across the arrays causes magnitude and phase

variations at the output antennas. It is believed that these variations contribute to creating different peak powers (316 and 513 mW), gains (2.1 and 6.5 dB), and far-field patterns. Additionally, differences in frequency response may be influenced by variations in slot antenna and CPW dimensions between the arrays due to variations in metallization and processing.

ACKNOWLEDGMENT

The authors thank J. Hubert and L. Mirth, Lockheed Martin, Orlando, FL, for the use of their hard horns and assistance throughout the project. The authors are also grateful to A. Mortazawi, S. Ortiz, and E. Schlecht for useful discussions.

REFERENCES

[1] R. York, "Quasioptical power combining," in *Active and Quasi-Optical Arrays for Solid-State Power Combining,* R. A. York and Z. B. Popović, Eds. New York: Wiley, 1997, ch. 1.

[2] Z. Popović and A. Mortazawi, "Quasi-optical transmit/receive front ends," *IEEE Trans. Microwave Theory Tech.,* vol. 46, pp. 1964–1975, Nov. 1998.

[3] J. Hubert, L. Mirth, S. Ortiz, and A. Mortazawi, "A 4-W Ka-band quasi-optical amplifier," in *IEEE MTT-S Int. Microwave Symp. Dig.,* June 1999, PP. 551–554.

[4] C. M. Liu, E. A. Sovero, W. J. Ho, J. A. Higgins, M. P. De Lisio, and D. B. Rutledge, "Monolithic 40-GHz 670-mW HBT grid amplifier," in *IEEE MTT-S Int. Microwave Symp. Dig.,* June 1996, pp. 1123–1126.

[5] M. P. De Lisio, S. W. Duncan, D. W. Tu, S. Weinreb, C. M. Liu, and D. B. Rutledge, "A 44-60 GHz monolithic pHEMT grid amplifier," in *IEEE MTT-S Int. Microwave Symp. Dig.,* June 1996, pp. 1127–1130.

[6] E. A. Sovero, J. B. Hacker, J. A. Higgins, D. S. Deakin, and A. L. Sailer, "A Ka-band monolithic quasi-optic amplifier," in *IEEE MTT-S Int. Microwave Symp. Dig.,* June 1998, pp. 1453–1456.

[7] M. A. Ali, S. Ortiz, T. Ivanov, and A. Mortazawi, "Analysis and measurement of hard horn feeds for the excitation of quasi-optical amplifiers," in *IEEE MTT-S Int. Microwave Symp. Dig.,* June 1998, pp. 1469–1472.

[8] M. Gouker, "Toward standard figures-of-merit for spatial and quasi-optical power-combined arrays," *IEEE Trans. Microwave Theory Tech.,* vol. 43, pp. 1614–1617, July 1995.

Todd Marshall (S'97) received the B.S. degree in engineering physics and the M.S. degree in electrical engineering from the University of Colorado, Boulder, in 1992 and 1996, respectively, and is currently working toward the Ph.D. degree in electrical engineering.

From 1993 to 1994, he developed numerical models of light-trapping in solar cells at the National Renewable Energy Laboratory. His research interests include Ka-band free-space power combiners and electromagnetic modeling.

Michael Forman (S'95) received the B.S.E.E. and M.S.E.E. degrees from the University of Colorado, Boulder, in 1996 and 1998, respectively, and is currently working toward the Ph.D. degree in electrical engineering.

His research interests include microwave and millimeter-wave power amplifiers, free-space power combiners, and K-band full-duplex amplifiers.

Zoya Popović (S'86–M'90–SM'99) received the Dipl.Ing. degree from the University of Belgrade, Yugoslavia, in 1985, and the Ph.D. degree from the California Institute of Technology, Pasadena, CA, in 1990.

She is currently an Associate Professor of electrical engineering at the University of Colorado, Boulder. Her research interests include microwave and millimeter-wave quasi-optical techniques, microwave and millimeter-wave active antennas and circuits, and RF photonics.

Dr. Popović received the IEEE Microwave Theory and Techniques Microwave Prize, the URSI Young Scientist Award, the National Science Foundation Presidential Faculty Fellow Award in 1993, and was awarded the International URSI Isaac Koga Gold Medal in 1996.